Journal of Hazardous Materials, 11 (1985) 261—279
Elsevier Science Publishers B.V., Amsterdam — Printed in The Netherlands

THE INITIAL AND GRAVITY-SPREADING PHASES OF HEAVY GAS DISPERSION: COMPARISON OF MODELS WITH PHASE I DATA

JAMES W. ROTTMAN, J.C.R. HUNT

Department of Applied Mathematics and Theoretical Physics, University of Cambridge, Silver Street, Cambridge CB3 9EW (Great Britain)

and A. MERCER

Safety Engineering Laboratory, Health and Safety Executive, Broad Lane, Sheffield S3 7HQ (Great Britain)

(Received July 20, 1984; accepted August 28, 1984)

Summary

The aim of this paper is to compare theoretical models with the observed behaviour of the heavy gas clouds in the Phase I Thorney Island field trials for small times after release. The approach we adopt is to divide the early-time motion into two phases: an initial phase, in which the motion is a strong function of the release conditions, and a gravity-spreading phase, in which motion is mainly horizontal and driven by buoyancy and the mean ambient flow. The results of idealised computations and experiments modelling these two phases are compared with the measurements and observations of the Phase I trials.

We find that in the initial phase, all the field trials are strongly buoyancy dominated, and therefore, that the flow field due to the containment vessel has only a minor effect on the initial motion of the cloud. The initial motion mostly consists of the generation of a radially spreading vortex ring. We perform idealised calculations that predict the time after release when this vortex ring is formed. In the gravity-spreading phase, we show that conventional gravity current theory fairly accurately describes the motion. As the ring expands, it leaves mixed fluid behind so that by the end of the gravity-spreading phase a fairly uniform well-mixed cloud remains. This is when "box-models" become the appropriate description. We also consider the effects of shear in the mean wind profile on the radially spreading gravity current. We show that shear is responsible for the upwind current front having the shape of a thin wedge and the downwind front having a thick shape with a nearly vertical leading edge. The behaviour of these two fronts explains the elongation of the cloud along the mean wind direction.

1. Introduction

Typically for the first 30 to 60 seconds after their release, the heavy gas clouds in the Thorney Island field trials dispersed under the action of the mean wind and their own buoyancy forces. Over this period atmospheric turbulence did not significantly affect their behaviour. This is the period we

consider in this paper. In particular, we seek an understanding of the effects of the release conditions used at Thorney Island on the subsequent dispersion of the heavy gas clouds. The approach we adopt, following [1], is to divide the motion for small and intermediate times after release into two phases: the initial phase, in which the motion is a strong function of the release conditions, and the gravity-spreading phase, in which the cloud spreads over the ground as a gravity current and is advected by the mean wind. We review the theories developed previously for these two phases and compare them with the mainly visual observations of the Phase I trials at Thorney Island.

2. The initial phase

As described more fully in [2] each experiment at Thorney Island was begun by releasing 2000 m^3 of a heavy gas nearly instantaneously from an approximately cylindrical container into an ambient wind. The heavy gas was usually twice the density of the surrounding air. The method for releasing the gas was to bring the sides of the container (made of plastic sheeting) rapidly to the ground with the assistance of elastic cords. This method was successful in producing an unconfined cylinder of heavy gas momentarily at rest in the ambient flow. Similar release methods have been used in the earlier field tests at Porton Down, described in [3], and in wind-tunnel simulations [4].

Immediately after the containment structure is removed, there are two forces acting on the heavy gas cloud: the drag force associated with the mean atmospheric flow around the containment structure and buoyancy force due to gravity and the density difference between the cloud and the surrounding air. An estimate of the relative magnitude of these two forces is given by a Richardson number, defined as

$$Ri_0 = g_0' h_0 / U_0^2 \tag{1}$$

where $g_0' = g(\rho_0 - \rho_a)/\rho_a$ is the reduced acceleration due to gravity, ρ_0 is the initial density of the released fluid, ρ_a is the density of the surrounding fluid, h_0 is the intial height of the cloud, and U_0 is a characteristic mean velocity of the ambient flow. For small values of this parameter, the motion is determined by the ambient flow and for large values by the buoyancy force.

For intermediate values of Ri_0 both forces will act simultaneously, but following [5] we consider for simplicity the two limiting cases of very small and very large Ri_0. This allows us to identify the different physical mechanisms that determine the motion of the cloud. As it turns out, the Thorney Island trials were all dominated by buoyancy forces in the initial phase, so they in fact correspond to the large Ri_0 limit.

2.1 $Ri_0 \ll 1$

For small values of Ri_0, the inital motion of the cloud is determined by the vorticity in the flow remaining from the interaction of the mean wind

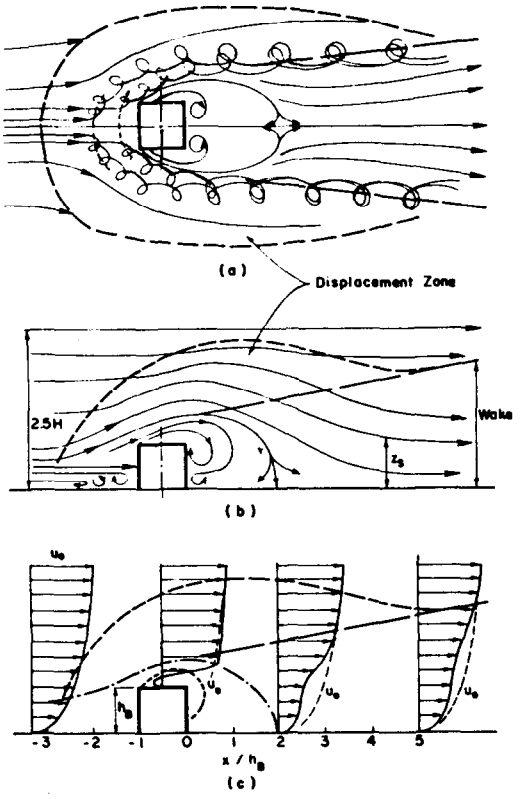

Fig. 1. Flow around a surface mounted cube based on smoke patterns in low speed wind tunnels: (a) plan view streamline pattern, (b) profile view streamline pattern, (c) profile view velocity profile, from [6].

with the containment structure. More specifically the vorticity shed from the structure and the ground *before* its collapse generates a flow that continues *after* the collapse. This flow for Reynolds numbers realised in the Thorney Island trials ($Re \approx 10^5$) is quite complicated. An idea of the flow structure is shown in the sketch in Fig. 1 (taken from [6]), which is based on observation of smoke patterns around surface mounted obstacles in low-speed wind tunnels. From the plan view, note the existence of a region of recirculating low-speed fluid directly downwind of the obstacle. Wrapped around the obstacle and its wake is a horseshoe-shaped vortex. This vortex begins upwind of the obstacle and its two legs trail downwind along the edges of the wake. Surface roughness or atmospheric turbulence can disrupt these structures so that they do not persist much beyond the downwind end of the recirculating region. From the side view, note that the flow accelerates over the top of the obstacle, reducing the pressure there, and attaches downwind.

A rough idea of what happens when the gas cloud is released in such a flow is illustrated in Fig. 2. The first sketch (Fig. 2a) shows the flow around

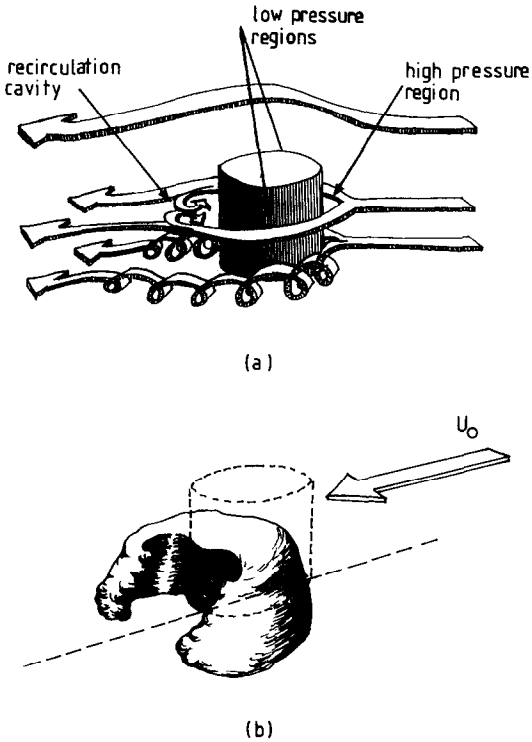

Fig. 2. Three-quarter view sketch of a column of gas at rest released in a cross flow: (a) before release, (b) just after release.

the containment vessel before it is removed. We have indicated in the sketch that the highest pressure is on the upwind side of the structure and the lowest pressure regions are on the two crosswind sides of the container. The pressure downwind is slightly less than the upwind pressure but greater than the pressure on the crosswind sides of the cylinder. The cloud just after release is sketched in Fig. 2b. The cloud spreads mostly in the crosswind direction, into the lowest pressure region. As it spreads in this direction, the surrounding flow tends to wrap the cloud around the recirculation region forming a horseshoe-shaped cloud when viewed from above. This description applies only to small Ri_0 releases, for large Ri_0 releases (as described in the next section) the cloud rapidly slumps to the ground with little influence from the surrounding flow.

Because the flow pattern around the containment structure is so complicated, it is difficult to determine in detail how the fluid in the recirculating region downwind, and the fluid contained in the structure accelerate after its removal. However, the essential features of the motion may be deduced from some idealised calculations. Consider a cylinder of neutrally buoyant fluid released instantaneously into a flow that is uniform far upwind. The potential flow calculation of this two-dimensional problem was

done numerically in [5] using a vortex-sheet method. Of course, the potential flow around a cylinder has no wake downwind of the cylinder. More recently, Rottman et al. [7] have used a vortex-in-cell method to compute numerically both the potential flow problem and the problem with a wake downwind of the cylinder (at a maximum Reynolds number of 500). In this latter calculation, the vortex-in-cell method was used to first compute the flow around the cylinder and then to compute the flow after the cylinder wall is removed.

Figure 3 shows the computed shapes of the released fluid for several times after release, as computed by the vortex-in-cell method, for both the case of potential flow and the case with $Re = 500$. In the potential flow calculation (Fig. 3a), the released fluid first elongated in the *crosswind* direction and then quickly rolls-up into a pair of counter-rotating vortices. Eventually ($t \approx 8r_0/U_0$, where r_0 is the initial cylinder radius and U_0 is the uniform speed of the ambient flow far upwind) the vortex pair forms a closed cell of fluid with approximately twice the area of the original cylinder. In the case with $Re = 500$ (Fig. 3b), a similar horseshoe-shaped contour is formed soon after release, but the contour never closes to form a closed cell of fluid. Apparently the released fluid is prevented from closing by the fluid that was in the wake downwind of the cylinder. Instead the released fluid is drawn out into a thin horseshoe shape, which if any turbulence were present would be broken up and dispersed.

Figure 4 is a plot of the computed speeds of the centres of mass of the released fluid for the two cases. In the potential flow case the speed increases to an approximately constant value of $0.8\ U_0$ in a time $t_a \approx 2r_0/U_0$, whereas in the case with $Re = 500$ the centre of mass accelerates more slowly but eventually attains the higher speed U_0 in a time $t_a \approx 5r_0/U_0$. For $Ri_0 \ll 1$, we define the end of the initial phase as the time t_a.

The laboratory experiments reported in [7] generally agree with the calculations for $Re = 500$, the same value for Re at which the experiments were made. The Reynolds numbers in the Thorney Island trials are, of course, much greater than 500, so the structure of the wake behind the containment structure is significantly different than in the calculations and in the laboratory experiments. In addition, the values of the Richardson numbers of the Thorney Island trials, except for Trials 1—4, are much too large for our low Richardson number description to be appropriate.

Neutrally buoyant fluid was released as a test of the equipment in Trials 1 and 2, and although no measurements were made, some video records were. The horizontal cross-section flows approximately correspond to the flow in Fig. 3 where the release structure has a downwind wake. It is interesting to note that these neutrally buoyant gas clouds actually lifted off the ground after release, appearing as if they were positively buoyant. This behvaiour is explained by considering the flow over the top of the containment structure. Since the flow is accelerated over the top, the pressure is decreased there causing the released fluid to initially rise.

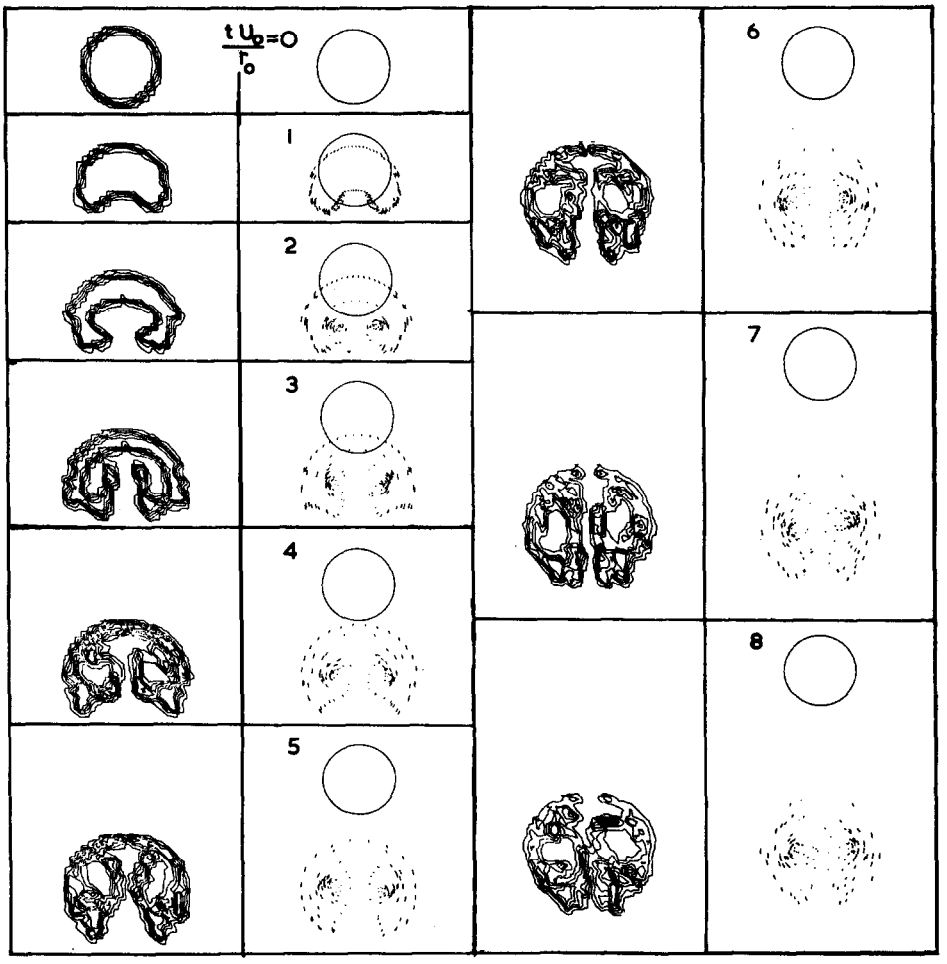

(a)

Fig. 3a. Computed shapes of a cylinder of fluid at rest released instantaneously in a uniform flow for the case of potential flow ($Re = \infty$), from [7]. The right-hand column in each figure shows the motion of the vortices on the edge of the released fluid over one time step. The left-hand column shows contours of concentration of particles marking the released fluid. The numbers indicate the time after release, non-dimensionalised by r_0/U_0.

The salient features of the types of motion we have been discussing here can be seen in a few of the large-Ri_0 Thorney Island trials, even though Ri_0 is large. As the dense cloud collapses downwards some mixing occurs, which leads to a small amount of the heavy fluid being left behind in the upper part of the region originally occupied by the cloud. This remaining fluid is quite dilute, and if the wind is strong enough a vortex sheet forms round this top section of the cylinder, which leads to it being carried downwind, above the main part of the cloud and rolling up into vortices. The best visualisation of this effect was obtained during one of the Phase II trials (Trial 24), because

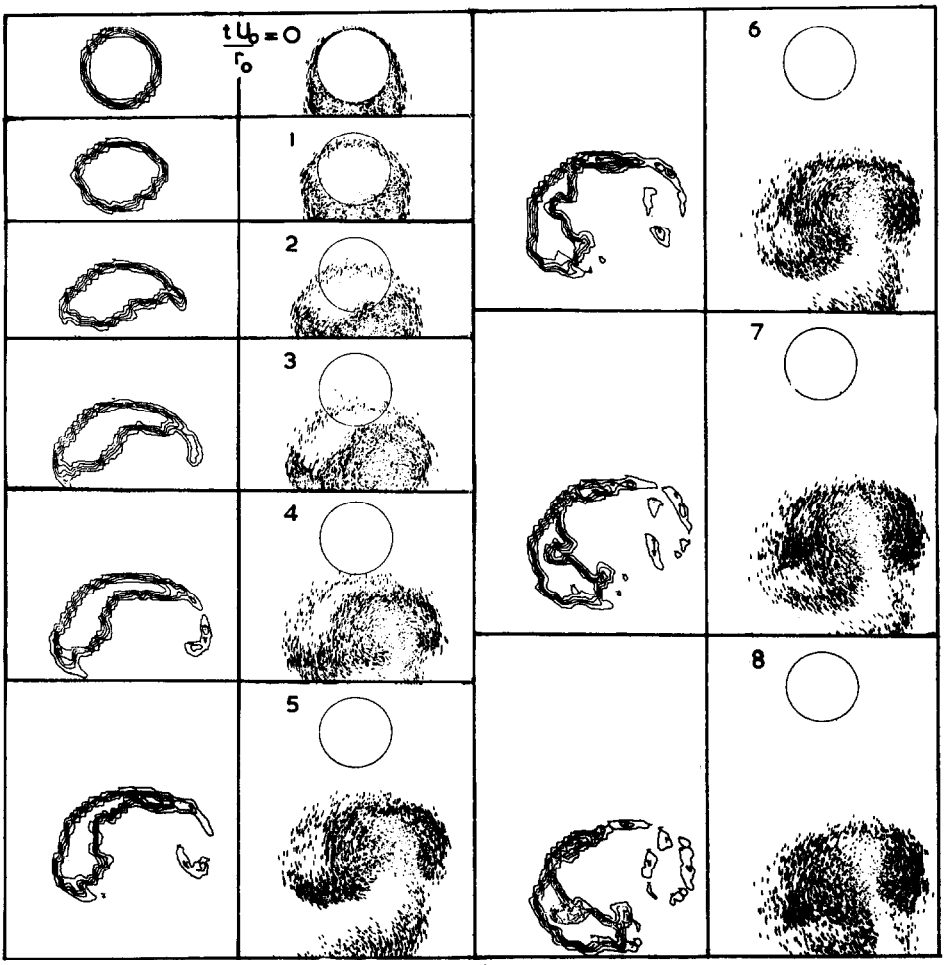

(b)

Fig. 3b. Computed shapes of a cylinder of fluid at rest released instantaneously in a uniform flow with $Re = 500$, from [7]. See also caption to Fig. 3a.

for some reason the smoke in the cloud initially occupied only the upper half of the containment vessel, making it easier to see the motion of the upper parts of the cloud from an overhead view. Figure 5 is an overhead photograph from Trial 24 that clearly shows the horseshoe-shaped structure (which has nothing to do with the horseshoe vortices generated by incident shear flow). This effect has also been observed by Hall [4] in regard to his wind tunnel simulations. His measurements show that the fluid transported downwind in the way we have described here is much less dense than the bulk of the cloud.

2.2 $Ri_0 \gg 1$

For large values of Ri_0 the cloud collapses symmetrically to the ground under its own buoyancy forces and the flow around the containment struc-

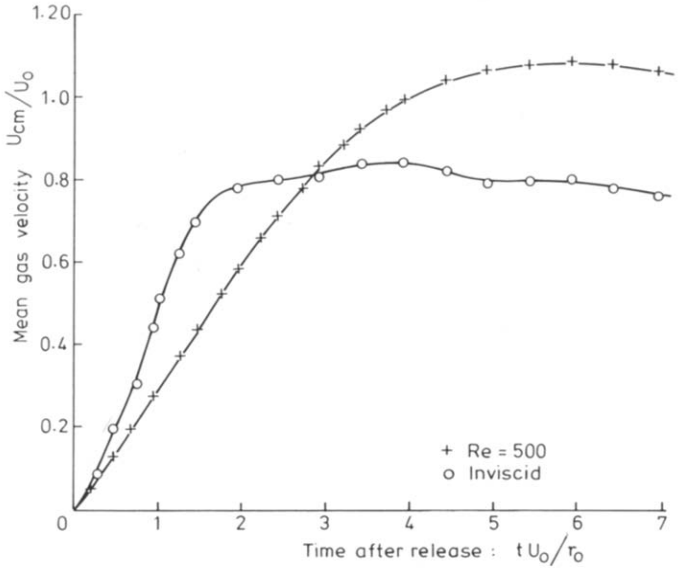

Fig. 4. The computed speeds of the centres of mass of a cylinder of fluid at rest released instantaneously into a uniform flow for the two cases: potential flow ($Re = \infty$) and flow with $Re = 500$, from [7].

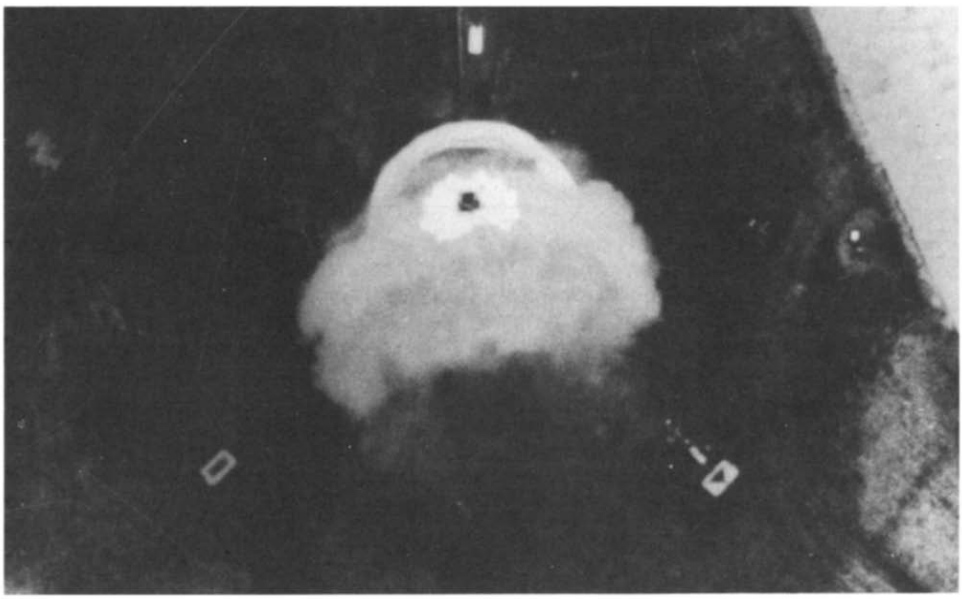

Fig. 5. An overhead photograph taken 4 seconds after release during Trial 24. The horse-shoe-shaped cloud of dilute gas is clearly visible above the bulk of the heavy cloud.

ture does not significantly affect the motion. As the cloud collapses, it spreads radially. The fluid in the cloud accelerates as it spreads radially except for the fluid near the current front. The front is inhibited from moving as fast as the following current of heavy fluid because it effectively experiences a "drag" caused by the inertia and shear stresses involved in accelerating the surrounding fluid. The net effect is the concentration of most of the heavy fluid in a narrow expanding ring. Note also that as the cloud collapses, vorticity is generated at the interface between the heavy fluid and the surrounding fluid (Fig. 7) which is then concentrated in the narrow expanding ring. Therefore, the ring is actually an expanding vortex ring, similar to a vortex ring that is approaching a wall. The time after release at which this

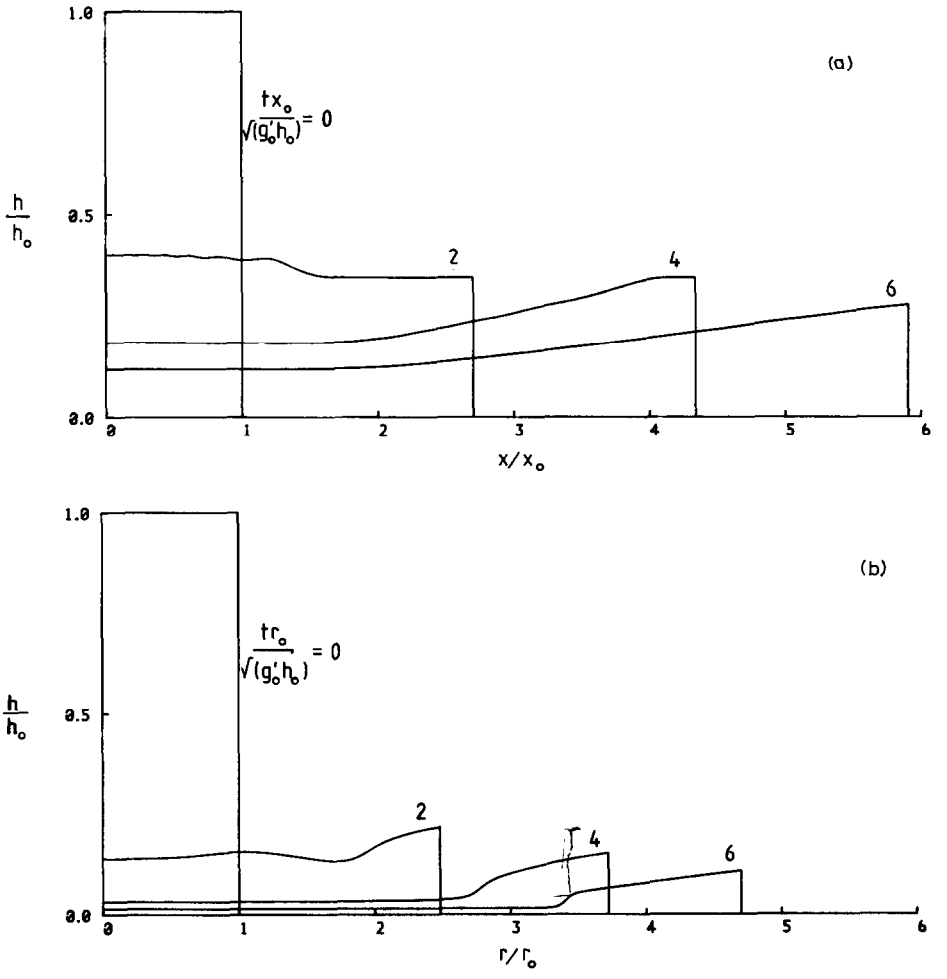

Fig. 6. The computed current depth profiles for the "dam-break" problem for several times after release: (a) plane flow, (b) axisymmetric flow.

vortex ring is established is what we define to be the end of the initial phase for large Ri_0.

The hydraulic calculations performed by Rottman and Simpson [5] of the "dam-break" problem give an estimate of the time after release at which the vortex ring is formed. The results of these calculations for the cross-sectional shape of the collapsing cloud for both plane and axisymmetric flow are shown in Fig. 6 for several times after release. In contrast to the plane flow case (Fig. 6a), the heavy fluid in the axisymmetric case (Fig. 6b) is mostly concentrated in an outer ring in a time $t_b \approx 4$—$6\ r_0/(g_0' h_0)^{1/2}$, which for the Thorney Island trials is about 4—6 seconds. These calculations are approximate, as they do not account for mixing between the two fluids nor are they able to describe the strong vortex motion at the current front. Nevertheless, they provide an approximation of the bulk motion of the cloud and have been shown (for example, [8]) to be very useful in predicting gravity current spreading rates. Measurements from the overhead and sideview video records of the Phase I trials taken with a stopwatch give fairly consistent results with $t_b \approx 6$ or 7 seconds for most of the trials, in good agreement with the numerical calculations. We note that the time required for the containment structure to be removed (≈ 2 seconds) is less than but comparable with t_b.

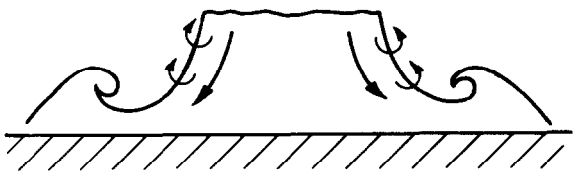

Fig. 7. Profile view sketch of a heavy gas column collapsing in still air, showing the generation of vorticity at the edges of the cloud.

The hydraulic calculations, which ignore vertical accelerations, cannot account for the observed strong vertical motion at the current front. The vorticity in this motion is generated at the edges of the cloud as it collapses vertically, as sketched in Fig. 7. Therefore, the scale and intensity of the motion in the spreading current front is determined by the initial *height* of the cloud. If the initial height of the cloud is greater or comparable to its initial diameter, then the could will be substantially mixed in the early stages of collapse. Thus, we would expect the dispersion of an initially tall and thin cloud to be more well mixed than an initially low and wide cloud. The released cloud in all the Thorney Island trials had an initial height comparable to its diameter, so that the initial mixing is significant in these trials. There is some evidence [9] that low, wide clouds may produce multiple concentric rings or concentric waves which may enhance mixing in these cases. But we have no clear explanation for these rings at the moment.

3. The gravity-spreading phase

As described in the previous section, buoyancy-dominated releases form a radially expanding vortex ring which contains most of the heavy fluid. When the ambient wind is small, this ring continues to expand nearly axisymmetrically. Vortex stretching tends to stabilize the ring and so the structure stays fairly coherent until sufficient energy is dissipated that the flow cannot be maintained. When this happens, the ring collapses. Since the expanding vortex ring leaves fluid behind as it grows, the heavy gas cloud has a roughly uniform mean concentration distribution, similar to that assumed in the commonly used box models of dense gas dispersion.

An estimate of the time t_c when the vortex ring collapses can be obtained from the numerical hydraulic calculations in [10]. Taking the time when the backward facing hydraulic jump disappears as the time when the ring collapses, we find that $t_c \approx 10t_b$, or about 60 seconds for most of the Phase I trials.

The time t_c for the Phase I trials was measured approximately from the video records using a stopwatch. We found that t_c is strongly dependent on the wind speed and also therefore on the wind shear and the intensity of the atmospheric turbulence. At low wind speeds, such as in Trials 7, 8 and 9, we measured $t_c \approx 45$ seconds, whereas at higher wind speeds we estimated $t_c \approx 20$ seconds. Our theoretical predictions are in fairly good agreement with the low wind trials, but clearly in the high wind cases other mechanisms have to be considered.

As the vortex ring expands, the heavy gas is mixed with the surrounding air much in the way described by Britter and Simpson [11]. This mixing leaves a layer of well-mixed gas behind the expanding ring that overlays a very thin layer of heavy gas. Therefore, at the time t_c when the vortex ring collapses, a fairly uniformly shaped, well-mixed cloud is left. This is the time at which "box models" become the appropriate description of the cloud.

3.1 Gravity spreading in an ambient flow

In a strong wind the cloud, after the initial collapse, is observed to elongate along the mean wind direction. It is observed that the upwind and downwind fronts move at different speeds and that the structure of these fronts is different. The upwind front is thinner and more wedge-shaped than a front moving into a fluid at rest and the downwind front is thicker and has a less distinct upper interface. These differences can be seen in the photograph of Trial 8 in Fig. 8, in which the upwind front is on the right-hand side of the photograph and the downwind front on the left-hand side.

Gravity current fronts moving in head or tail winds have been studied in the laboratory by Simpson and Britter [12]. They found that their laboratory data as well as the available atmospheric data are described by the empirical formula

$$U_f/U_0 = 0.91 + 0.62\,\bar{U}/U_0$$

Fig. 8. Profile view photograph of Trial 8 at 18 seconds after release. The upwind front at the right is wedge-shaped, as in Fig. 9a and the downwind front at the left is nearly vertical, as in figure 9c.

where U_f is the front speed, $\bar{U}$ is some mean wind speed, $U_0 = (g'h)^{1/2}$, g' is the reduced acceleration due to gravity, and h is the thickness of the gravity current. If the ambient wind simply advected the gravity current, with no changes to the structure of the front, the coefficient of $\bar{U}/U_0$ would be unity. Clearly, we conclude that the wind affects the front structure and consequently the front speed *relative* to the wind.

Shadowgraphs from [12] of laboratory gravity currents in uniform, headwind and tailwind flows are shown in Fig. 9. Sketches of the velocity profiles for the different ambient flows are shown on the left of the figure. The structure of these laboratory current fronts compare qualitatively quite well with the upwind and downwind fronts in Fig. 8. It was observed in the experiments that the stability of the fronts were quite different. The upwind front appeared to be fairly stable with much less mixing than a front moving into a uniform flow, and the downwind front appeared less stable with more mixing. These different mixing characteristics of the two probably account for their different speeds relative to the wind.

By a simple idealised analysis, we can show that the different front shapes might also be caused by shear in the ambient wind. Our inviscid analysis, which is described in detail in the Appendix, is basically the same as von Karman's [13] theory for the shape of the leading edge of the front except that we include the additional possibility of shear in the approach flow. The theory of von Karman predicts that a two-dimensional gravity current that

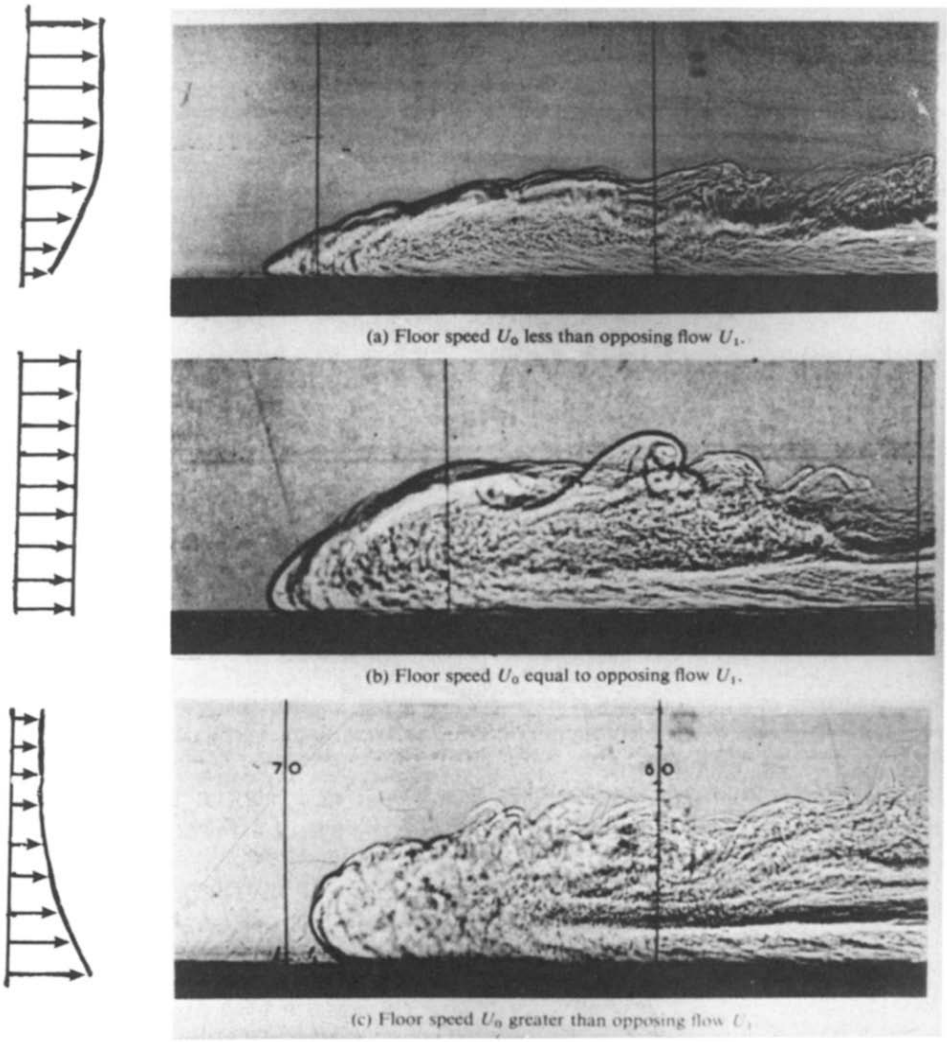

Fig. 9. Shadowgraph of two-dimensional gravity current heads: (a) in a headwind (positive shear), (b) in uniform flow, (c) in a tailwind (negative shear). The sketches at the left indicate the shear profile relative to the front in each case. From [12].

propagates steadily into a fluid at rest has a leading edge that encloses an angle of 60°, as sketched in Fig. 10a. With shear in the approach flow, our analysis shows that the leading edge is either thinner or thicker than the no-shear solution depending on the type of shear. In a reference frame in which the gravity current front is at rest, the front is thinner if the oncoming flow increases with height above the ground (as sketched in Fig. 10b) and is thicker if the oncoming flow decreases with height (as sketched in Fig. 10c).

We are concerned here with how well the clouds in the Thorney Island

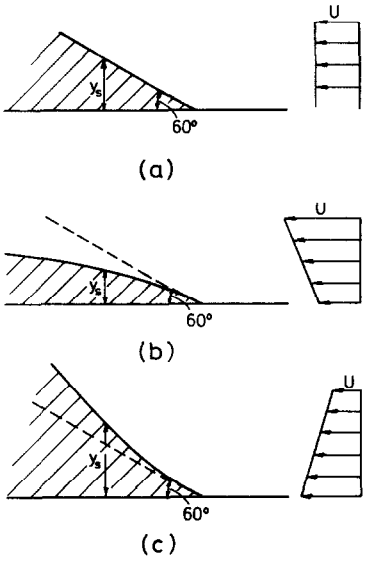

Fig. 10. Sketch of a steady two-dimensional gravity current front moving into different shear flows in a reference frame in which the front is at rest: (a) uniform ambient flow, (b) headwind, (c) tailwind.

trials conform with the above empirical formula. To do this we estimated the upwind and downwind front speeds from the tracings [14] of the overhead photographs of the Phase I trials.

Figure 11 is a typical tracing (the particular case shown is Trial 14) at some time after release. The visible outline of the cloud is marked by a heavy

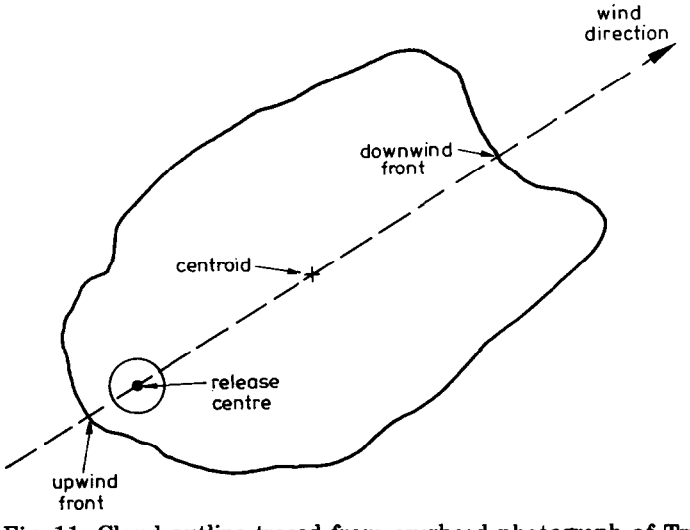

Fig. 11. Cloud outline traced from overhead photograph of Trial 14 at 25 seconds after release.

black line, the release centre by a black dot, and the centre of gravity of the cloud by a +. A dashed straight line through the release centre and the centre of gravity is nearly parallel to the mean wind direction. We define the upwind front as the intersection of this dashed line with the cloud outline on the upwind side of the release centre, and similarly we define the downwind front as the intersection on the downwind side. In this manner, the distances of the upwind and downwind fronts from the release centre were measured from each frame of the overhead photographic record.

Figure 12 is a plot of these front positions as well as the centroid positions as a function of time after release for Trial 8. This plot is typical of all the plots of this type that we made and they lead to a number of interesting conclusions. The clouds always begin by collapsing symmetrically, which is evidence for the strongly buoyancy dominated character of the initial phase of collapse. But in a time dependent on the strength of the wind the upwind and downwind fronts attain different constant speeds, the upwind front travelling more slowly. Eventually, the upwind front comes to rest and seems to remain stationary, probably being eroded from the top. Once the upwind front comes to rest, the centroid attains a fairly uniform speed in the downwind direction.

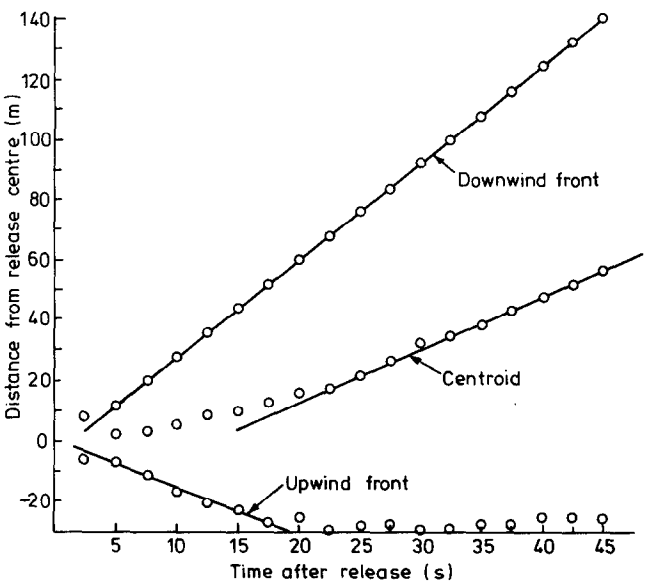

Fig. 12. Plots of the positions of the upwind and downwind fronts and the cloud centroid as functions of time after release, for Trial 8.

We estimated the speeds of the upwind and downwind fronts by fitting straight lines to the plots of their positions versus time and measuring the slopes of these lines. Figure 13 is a plot of the speeds so attained versus the mean wind speed at 10 m above the ground. Also plotted is the line repre-

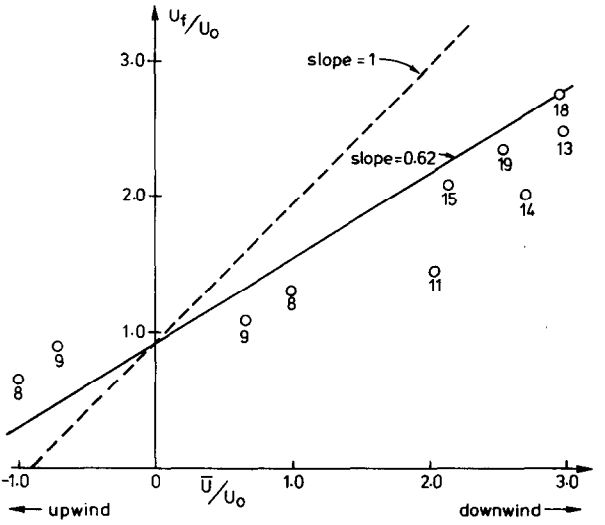

Fig. 13. A plot of the upwind and downwind front speeds as functions of the mean wind speed at 10 m above the ground. The numbers next to each data point identify the trial. The solid line represents the empirical formula developed in [12] and the dashed line is a straight line with unit slope.

senting the emprical formula. The agreement is acceptable; the data are certainly better correlated by this formula than by the naive theory with unity slope (represented by a dashed line in the plot).

4. Conclusions

In comparing some idealised models of the initial and gravity-spreading phases with the Phase I trials at Thorney Island, we can draw a number of conclusions about the effects of the particular initial conditions used in the field trials. First, the Phase I trials, except for the first four test trials, were all strongly buoyancy dominated. Because of this, the primary mixing mechanism in the initial phase is the formation of a radially expanding vortex ring. We have given an explanation for how this ring forms and time scales for its formation. The structure of the cloud, and hence the initial dilution, is strongly dependent on the aspect ratio of the initial cloud. The strength and width of the ring scale on the initial height. So, the Thorney Island trials with a unity aspect ratio cloud is much more mixed, initially, than a low, wide cloud. We have also given an estimate of when "box-models" become the appropriate description of the cloud.

The gravity-spreading phase seems to be well described by standard gravity current theory. We have shown that shear in the mean ambient flow plays an important role in determining the amount of mixing in the gravity current fronts and in determining the different speeds of the upwind and downwind fronts.

Acknowledgement

This work was supported by the U.K. Health & Safety Executive under contract 1918/01.01. We are grateful for informative discussions with Dr. R.E. Britter and Dr. J.E. Simpson. We also thank A.J. Prince for providing us with her cloud tracings from the overhead photographs of the Phase I trials.

British Crown Copyright 1985.

References

1 J.C.R. Hunt, J.W. Rottman and R.E. Britter, Some physical processes involved in the dispersion of dense gases, in: G. Ooms, H. Tennekes (Eds.), Atmospheric Dispersion of Heavy Gases and Small Particles, Proc. IUTAM Symposium, Delft, The Netherlands, 1983, Springer-Verlag, Berlin, 1984.
2 D.R. Johnson, Thorney Island trials: systems development and operational procedures, J. Hazardous Materials, 11 (1985) 35—64.
3 R.G. Picknett, Dispersion of dense gas puffs in the atmosphere at ground level. Atmos. Environ., 15 (1981) 509—525.
4 D.J. Hall and R.A. Waters, Wind tunnel model comparisons with the Thorney Island dense gas release field trials, J. Hazardous Materials, 11 (1985) 209—235.
5 J.W. Rottman and J.E. Simpson, The initial development of gravity currents from fixed-volume releases of heavy fluids, in: G. Ooms, H. Tennekes (Eds.), Atmospheric Dispersion of Heavy Gases and Small Particles, Proc. IUTAM Symposium, Delft, The Netherlands, 1983, Springer-Verlag, Berlin, 1984.
6 R.N. Meroney, Turbulent Diffusion Near Buildings, in: E. Plate (Ed.), Engineering Meteorology, Elsevier, Amsterdam, 1982, p. 484.
7 J.W. Rottman, J.E. Simpson and P.K. Stansby, The motion of a two-dimensional cloud released instantaneously in a uniform cross flow, to be published.
8 J.W. Rottman and J.E. Simpson, Gravity currents produced by instantaneous releases of a heavy fluid in a rectangular channel, J. Fluid Mech., 135 (1983) 95—110.
9 T.O. Spicer and J.A. Havens, Modelling the Phase I Thorney Island experiments, J. Hazardous Materials, 11 (1985) 237—260.
10 R.E. Grundy and J.W. Rottman, The approach to self-similarity of the solutions of the shallow-water equations representing gravity current release, to be published.
11 R.E. Britter and J.E. Simpson, Experiments on the dynamics of a gravity current head, J. Fluid Mech., 88 (1978) 223—240.
12 J.E. Simpson and R.E. Britter, A laboratory model of an atmospheric mesofront, Q.J. Roy. Met. Soc., 106 (1980) 485—500.
13 T. von Karman, The engineer grapples with nonlinear problems, Bull. Amer. Math. Soc., 46 (1940) 615—683.
14 P.W.M. Brighton, A.J. Prince and D.M. Webber, Determination of cloud area and path from visual and concentration records, J. Hazardous Materials, 11 (1985) 155—178.

Appendix

Here we give a mathematical treatment of the shape of a gravity current front that is moving into a shear flow. In a coordinate system fixed with the front of the current, the upwind flow is $U = U_0 + \omega y$, as sketched in Fig. 14a. Then we consider the solution of the equations

$$\nabla^2\psi_1 = 0, \qquad \nabla^2\psi_2 = -\omega,$$

where ψ_1, ψ_2 are the stream functions in the current and outside the current, respectively, and ω is the vorticity in the external flow. The kinematic boundary conditions are

$$\begin{aligned} \psi_1 &= 0 \qquad \text{on } \theta = \pi \\ \psi_2 &= 0 \qquad \text{on } \theta = 0 \\ \psi_1 = \psi_2 &= 0 \qquad \text{on } \theta = \theta_s(r) \end{aligned}$$

where $\theta_s(r)$ describes the interface between the current and the external flow. On this interface we also have the dynamic boundary condition

$$\frac{1}{2}(u_2^2 + v_2^2) - g'y_s = \frac{1}{2}\frac{\rho_1}{\rho_2}(u_1^2 + v_1^2),$$

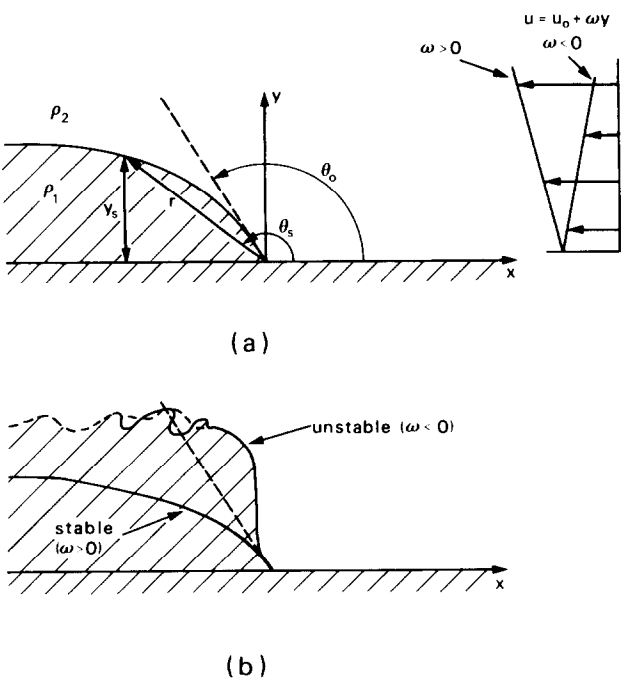

Fig. 14. Inviscid analysis of the shape of a gravity current front moving into a shear flow: (a) co-ordinate system, (b) computed shapes for the two cases of the current moving into a head wind ($\omega > 0$) and into a tail wind ($\omega < 0$).

where u, v are the horizontal and vertical velocities and y is the vertical coordinate.

We seek solutions that are valid near the front of the gravity current and so take ω to be constant and expand ψ_1, ψ_2 and θ_s in power series in r. Substituting these expansions into the governing equations and choosing the solutions that satisfy the boundary conditions to $O(r^2)$ we find

$$\theta_s(r) = \frac{2\pi}{3} + 3^{-1/4}\frac{\omega r^{1/2}}{(g')^{1/2}}$$

$$\psi_1 = 0$$

$$\psi_2 = -\frac{1}{4}\omega r^2(1 - \cos 2\theta) - 2(3)^{-3/4}(g')^{1/2} r^{3/2} \sin\left(\frac{3}{2}\theta\right) + \frac{5\omega}{4\sqrt{3}} r^2 \sin(2\theta)$$

The solution for $\theta_s(r)$ shows that when $\omega > 0$ (headwind) $\theta_s(r)$ increases with r away from the potential flow solution ($\theta_s(r{=}0) = 2\pi/3$) and for $\omega < 0$ (tailwind), $\theta_s(r)$ decreases with r. This implies that a gravity current front moving into a headwind with shear is thinner than without shear and conversly a front moving with a tailwind with shear is thicker. These different cases are sketched in Fig. 14b.